An Accurate Mathematical Approach for Calculating Capillary Pressure in Drainage and Imbibition from Centrifuge Data

Hossein Beyrami, Ehsan Kamari*

Department of Petroleum Engineering, Research Institute of Petroleum Industry, Tehran, Iran

* Corresponding author: kamarie@ripi.ir; Cell phone +98 912 4147996.

Abstract

The conversion of centrifuge data into capillary pressure curves is crucial for rock capillary pressure measurement in various applications. This process involves converting measured fluid productions into local saturation values, and the accuracy and efficiency of this procedure are essential. This paper addresses the challenge of achieving accuracy without sacrificing computational efficiency by introducing a new method based on the Reproducing Kernel Hilbert Space (RKHS) technique. This approach enables the conversion of capillary pressure versus average saturation data into capillary pressure versus local (outlet) saturation. The RKHS method is applied to both drainage and imbibition centrifuge data, and its efficiency and accuracy are evaluated using both artificially generated and experimental datasets. The results obtained with the RKHS method are compared and validated against other existing methods.

Keywords: Drainage, Imbibition, Capillary pressure, RKHS method, Singular integral equation

1. Introduction

Capillary pressure curves are extensively used in the petroleum industry, such as two and three-phase fluid flow simulation in porous media, making decisions about enhanced oil recovery (EOR) management, determining rock wettability, and estimating pore size distribution [**Error! Reference source not found.**–7]. The equation for centrifuge capillary pressure represents a singular integral equation, and researchers have proposed various approximate solutions to this equation [8, 9]. Recently, Bursey et al. [10] even employed machine learning techniques for predicting centrifuge capillary pressure.

In centrifuge experiments, average saturation $\bar{S}$ is measured against capillary pressure Pc_1 at the inlet face of a rock sample during rotation at various angular velocities ω (Figure 1). Hassler and Brunner [11] and Hermansen et al. [12] established the relationship between average saturation $\bar{S}(Pc_1)$ and local saturation $S(Pc)$. Their assumptions include hydrostatic equilibrium in each phase and Dirichlet boundary condition of $Pc = 0$ at the outflow. Capillary pressure can be measured at any distance (r) from the centrifuge axis for drainage experiments using the following equation:

$$Pc_r = \frac{1}{2}\Delta\rho\omega^2(r_2^2 - r^2), \tag{1.1}$$

Where:

- Pc_r is the capillary pressure at radius r .
- $\Delta\rho$ is the difference between the phase densities.

- ω is the rotation speed.
- r_1 and r_2 are the radii at the core faces having minimum and maximum distance from the center, respectively.

Based on Eq. (1.1), capillary pressure at the face near the center is:

$$Pc_1 = \frac{1}{2}\Delta\rho\omega^2(r_2^2 - r_1^2). \tag{1.2}$$

Using Eqs. (1.1) and (1.2), we have:

$$Pc = Pc_1 \frac{(r_2^2 - r^2)}{(r_2^2 - r_1^2)}. \tag{1.3}$$

The proportion between S and its average is:

$$\bar{S} = \frac{1}{(r_2 - r_1)}\int_{r_1}^{r_2} S(r)dr. \tag{1.4}$$

Finally, the following equation can be derived after mathematical calculation:

$$\bar{S}(Pc_1) = \frac{r_1 + r_2}{2\sqrt{Pc_1}}\int_0^{Pc_1} \frac{S(Pc)}{\sqrt{r_2^2 Pc_1 - (r_2^2 - r_1^2)Pc}}dPc, \tag{1.5}$$

or

$$\bar{S}(Pc_1) = \frac{r_1 + r_2}{2r_2\sqrt{Pc_1}}\int_0^{Pc_1} \frac{S(Pc)}{\sqrt{Pc_1 - BPc}}dPc, \tag{1.6}$$

where

$$B = 1 - \left(\frac{r_1}{r_2}\right)^2,\ 0 \le B \le 1. \tag{1.7}$$

For imbibition experiments, similar equations are obtained exchanging r_1 for r_2,

$$B = 1 - \left(\frac{r_2}{r_1}\right)^2, \tag{1.8}$$

and Pc_1 for Pc_2, where Pc_2 is the capillary pressure at radius r_2 [13, 1312]. Both drainage and imbibition experiments, capillary pressure ($S(Pc)$) aim to obtain from centrifuge data ($\bar{S}(Pc_1)$) using Eq. (1.6).

Various methods have been proposed to approximate the solution of Eq. (1.6). Hassler and Brunner (HB) assumed that the pressure field in the core is linear and the gravity has no influence on the pressure field [14]. These assumptions are valid for narrow and short samples inside a centrifuge with a long rotational axis. So, this method gives smaller saturations compared to the exact solution [15]. The Hoffman method [16], van Domselaar method [17], Rajan method [18], Forbes methods [19], and Nazari Moghaddam [20] address the solution of fundamental Eq. (1.6). It is revealed that all mentioned methods use a simplified version of Eq. (1.6). It is because the weakly singular Volterra integral Eq. (1.6) is known to be ill-conditioned [11, 12]. In other words, error in local saturation increases during inverting noisy average saturation data. In this regard, various interpretation

procedures were carried out [15, 21, 22]. However, for better accuracy, these methods need special experimental facilities. Forbes methods have simple implementation but are sensitive to pressure step size and give fluctuated results [19]. Except for the Forbes methods, other mentioned methods such as Nazari Moghaddam (NM) and Hassler and Brunner (HB) address the solution of only drainage experiments. Considering the numerous industrial applications of the centrifuge technique, a robust method that provides accurate results with less computational time is still demanded in both drainage and imbibition experiments.

In this paper, reproducing kernel Hilbert space (RKHS) method is introduced for solving the fundamental centrifuge equation (Eq. (1.6)) to obtain local saturation from centrifuge data for both drainage and imbibition experiments.

2. RKHS Method

The theory of reproducing kernel, initially introduced by Zaremba [23], has been widely used to solve boundary value problems [24]. Aronszajn [25] further developed the theory, introducing Bergman kernel functions that have found applications in solving various problems. Cui and Lin [26], after summarizing RKHS theory, have solved different problems. Karatas Akgül [27] has proposed the RKHS method for nonlinear boundary-value problems. Foroutan et al. [28] used the RKHS method for computing solutions of nonlinear third-order ordinary differential equations under multipoint boundary conditions. Recently, the RKHS method has been used to address problems across different scientific domains [29−36].

Fundamentally, the centrifuge equation (Eq. (1.6)) can be rearranged as follows:

$$F(Pc_1) = \int_0^{Pc_1} K(Pc_1, Pc) S(Pc) dPc, \quad Pc_1 \geq 0, \tag{2.1}$$

where

$$F(Pc_1) = \frac{2r_2}{r_1 + r_2} \left[\bar{S}(Pc_1) \sqrt{Pc_1} \right], \tag{2.2}$$

and

$$K(Pc_1, Pc) = \frac{1}{\sqrt{Pc_1 - B\ Pc}}. \tag{2.3}$$

Above equation can be rewritten as

$$f\ (Pc_1) = \int_0^{Pc_1} K(Pc_1, Pc) s(Pc) dPc, \quad 0 \leq Pc_1 \leq 1, \tag{2.4}$$

where

$$f(Pc_1) = \frac{1}{\sqrt{Pc_{\max}}} F(Pc_{\max}\ Pc_1), \tag{2.5}$$

and

$$s(Pc_1) = S(Pc_{\max}\ Pc_1). \tag{2.6}$$

$Pc_{\max}$ is defined as the maximum capillary pressure data that centrifuge experiments are conducted. The space $W^{m}[0,1]$ is defined as follows:

$$W^{m}[0,1]=\left\{s(x)\,|\,s^{(m-1)}(x)\in AC[0,1],\ s^{(m)}(x)\in L^{2}[0,1]\right\}, \tag{2.7}$$

where $AC[0,1]$ stands for an absolutely continuous real-valued function on $[0,1]$. The following concepts:

$$(s,q)_{m}=\sum_{i=0}^{m-1}s^{(i)}(0)q^{(i)}(0)+\int_{0}^{1}s^{(m)}(x)q^{(m)}(x)dx, \tag{2.8}$$

and

$$\|s\|_{m}=\sqrt{(s,s)_{m}},\quad s,q\in W^{m}[0,1], \tag{2.9}$$

are the inner product and norm in $W^{m}[0,1]$ respectively. $W^{m}[0,1]$ is a complete Hilbert space and contains a unique reproducing kernel function [37]. Therefore, $W^{m}[0,1]$ is defined as a reproducing kernel Hilbert space. Let $R_{x}^{m}(y)$ denote the reproducing kernel of $W^{m}[0,1]$. For every $s\in W^{m}[0,1]$ and fixed $x\in[0,1]$, $R_{x}^{m}(y)$ satisfies the following reproducing property:

$$s(x)=(s(y),R_{x}^{m}(y))_{m}. \tag{2.10}$$

For more detail of $R_{x}^{m}(y)$ calculation see the Appendix. $R_{x}^{1}(y)$ is as follow

$$R_{x}^{1}(y)=\begin{cases}1+y, & y\le x,\\ 1+x, & y>x.\end{cases} \tag{2.11}$$

For $\{x_{j}\}_{j=1}^{n}$, $x_{j}\in[0,1]$, we define

$$\psi_{j}(x)=R_{x}(x_{j})+\int_{0}^{x_{j}}K(x_{j},t)R_{x}(t)dt. \tag{2.12}$$

An orthonormal system of $\{\bar{\psi}_{j}\}_{j=1}^{n}$ is derived by applying the Gram–Schmidt orthogonalization process on $\{\psi_{j}\}_{j=1}^{n}$. In other words:

$$\bar{\psi}_{j}(x)=\sum_{k=1}^{j}\beta_{jk}\psi_{k}(x), \tag{2.13}$$

where β_{jk}, $k=1,2,\ldots,j$, are the Gram–Schmidt orthogonalization coefficients. The approximate solution of (2.4) can be written as:

The approximate solution of Eq. (2.4) can then be written as:

$$s_{n}(x)=\sum_{j=1}^{n}\sum_{k=1}^{j}\beta_{jk}f(x_{k})\bar{\psi}_{j}(x). \tag{2.14}$$

For detailed computational procedures and proof, readers are referred to Beyrami et al. [24] and the provided appendix.

3. Results and Discussion

Two sets of examples are used in this study. The first step (validation part) was an accuracy assessment on an artificially generated dataset. These examples have exact solutions reported in the literature and are used for error analysis and validation [19, 20]. Different numbers of data points are used to demonstrate the convergence of the approximate solution to the theoretical function as the data points increased. The results of the different values of B are used to consider the effect of B on the approximate solution of the RKHS method. The next two sets of experimental centrifuge data were used to consider the performance of the RKHS method. The next two sets of experimental centrifuge data that contains capillary pressure versus average saturation, were used to consider the performance of the RKHS method. These examples lack exact responses and error evaluation cannot be done for them. Therefore, these examples are presented as case studies for practical application.

3.1. Validation

In this section, the applicability of the proposed method is tested on artificially generated datasets for both drainage and imbibition experiments. Moreover, the accuracy is evaluated and compared with the methods from the literature for different numbers of experimental data points and the values of B . Forbes's second method is believed to be the most accurate and simple method [19]. Therefore, in the following figures, the RKHS method is compared with the Forbes method, and comparison results with other methods are presented in tables. For this purpose, the root mean square error (RMSE) and the relative error with the following definitions

$$RMSE = \sqrt{\frac{\sum_{i=1}^{n}(S_{theoretical,i} - S_{predicted,i})^2}{n-1}}, \quad RelativeError = \frac{\left|S_{theoretical} - S_{predicted}\right|}{\left|S_{theoretical}\right|}, \qquad (3.1)$$

are reported in the tables and figures, respectively. Used functions are assumed to be the exact local capillary function or saturation function $S(Pc_1)$. Using Eq. (1.6), the centrifuge data that are average saturation, $\bar{S}(Pc_1)$, are artificially obtained. Predicted local saturation function $S_{n,B}(Pc_1)$ for different values of n and B are obtained by (2.14) as $S_{n,B}(Pc_1) = s_{n,B}(Pc_1 / Pc_{\max})$.

Example D1: The following function is used for drainage experiments as the exact theoretical local saturation by Forbes [19] and Nazari Moghaddam [20]:

$$S(Pc) = \begin{cases} 1, & 0 < Pc \le 2, \\ \dfrac{1.5}{Pc} + 0.25, & Pc > 2. \end{cases} \qquad (3.2)$$

Example D2: The following function is used for drainage experiments as the exact theoretical local saturation by Nazari Moghaddam [20]:

$$S(Pc) = \begin{cases} 1, & 0 < Pc \le 0.25, \\ \dfrac{0.5}{\sqrt{Pc}}, & Pc > 0.25. \end{cases} \qquad (3.3)$$

Example D3: The following function is used for drainage experiments as the exact theoretical local saturation by Forbes [19]:

$$S(Pc) = 0.1 - 0.9\, Exp(-1.66Pc + 0.083). \tag{3.4}$$

Figures 2, 3, and 4 illustrate the solution and the relative error of the RKHS method for $B = 0.75$ and the varying numbers of data points for the drainage experiment. The derived solution converges to the precise answer as the number of data points grows. Figures 5a, 6a, and 7a show the comparison result of RKHS and the Forbes method with the precise theoretical $S(Pc)$ for $B = 0.75$ and $n = 10$ data points for the drainage experiment. Figures 5b, 6b, and 7b indicate the interpretation of $S_B(Pc)$ and $\bar{S}_B(Pc_1)$ for n=50 data points and B=0.1, 0.5, 0.8, 0.95, and 1 for the drainage experiment. As a result, the RKHS method has good accuracy for different values of B. Table 1 also presents the superior results of the RKHS method for drainage experiments versus the Hassler and Brunner (HB) solution [14] and the Nazari Moghaddam (NM) solution [20]. The RMSE values for drainage examples D1, D2, and D3 stand at 4.19E-3, 0.031, and 0.031, respectively, marking them as the lowest values among the compared methods. As shown, the RKHS method is more accurate than the other methods.

Example I1: The following function is used for imbibition experiments as the exact theoretical local saturation by Forbes [19]:

$$S(Pc) = \begin{cases} 0.1, & 0 \geq Pc \geq -0.001, \\ 0.1 + 0.1\, Log(-1000\, Pc), & Pc < 0.001. \end{cases} \tag{3.5}$$

Example I2: The following function is used for imbibition experiments as the exact theoretical local saturation by Forbes [19]:

$$S(Pc) = 0.85 + 1.5/(Pc - 2). \tag{3.6}$$

Figures 8 and 9 illustrate the solution and the absolute error of the RKHS method for $B = -4.0$ and the different numbers of data points for the imbibition experiment. As the number of data points rises, the resultant solution converges to reliable response. Figures 10a and 11a demonstrate the comparative result of RKHS and Forbes methods with exact theoretical $S(Pc)$ for $B = -4.0$ and $n = 10$ data points for the imbibition experiment. Figures 10b and 11b indicate interpretation of $S_B(Pc)$ and $\bar{S}_B(Pc_1)$ for n=50 data points and B=-0.1, -1, -4, -20, and -100 for imbibition experiment. Therefore, the RKHS method has good accuracy for different values of B. Table 2 also presents the RMSE superior results of the RKHS method for imbibition experiments versus the Forbes method solution [19]. As shown, for imbibition examples I1 and I2, the RMSE values are 9.41E-3 and 7.29E-3, both of which are lower than the error associated with the Forbes method.

3.2. Case Study

In this section, two sets of experimental centrifuge data for drainage and imbibition experiments are used to compare the RKHS method with the Forbes method [19]. Figures 12a and 12b illustrate the following fitted curve:

$$\bar{S}(Pc) = \frac{a\, Pc^b + c}{d\, Pc^e + f}. \tag{3.7}$$

with experimental centrifuge data $\bar{S}$, based on RKHS and Forbes methods for each case study. RKHS and Forbes methods are compared using interpolated $\bar{S}$ data. The results of this comparison showed the robustness and accuracy of the RKHS method across different cases.

Example D4: A set of experimental centrifuge data $\bar{S}$ for drainage experiment is used to compare the RKHS method with the Forbes method [19]. The rock sample properties are in Table 3.

Example I3: A set of experimental centrifuge data $\bar{S}$ for the imbibition experiment is used to compare the RKHS method with the Forbes method [19]. Table 4 contains the rock sample properties.

4. Conclusions

In this paper, the solution of the fundamental centrifuge equation is derived using the RKHS method. The proposed method provides an accurate and efficient solution for calculating capillary pressure from centrifuge data. The accuracy of the RKHS method is validated and compared with other methods using both artificially generated and experimental data. The method demonstrated its versatility and computational efficiency across a range of B values, offering a promising solution for analyzing experimental results in both drainage and imbibition studies. The results obtained with the RKHS method exhibited significantly higher precision compared to the other methods.

Appendix

This section includes computational details based on the RKHS theory. The provided appendix presents the nomenclature and mathematical procedures used in the calculations. Suppose that R_y denote the reproducing kernel function of $W^m[0,1]$. By the definition of reproducing property in Eq. (2.10), for every $y \in [0,1]$ and $s \in W^m[0,1]$, we have

$$s(y) = (s(x), R_y^m(x))_m. \tag{A.1}$$

By Eq. (2.10), the definition of inner product in $W^m[0,1]$, we have

$$(s, R_y)_m = \sum_{i=0}^{m-1} s^{(i)}(0) R_y{}^{(i)}(0) + \int_0^1 s^{(m)}(x) R_y{}^{(m)}(x) dx, \tag{A.2}$$

Using integration by parts m times, we can get

$$\int_0^1 s^{(m)}(x) \frac{\partial^m R_y(x)}{\partial x^m} dx = \sum_{i=0}^{m-1} (-1)^i s^{(m-i-1)}(x) \frac{\partial^{m+i} R_y(x)}{\partial x^{m+i}} |_{x=0}^1 + (-1)^m \int_0^1 s(x) \frac{\partial^{2m} R_y(x)}{\partial x^{2m}} dx, \tag{A.3}$$

and after a change of variable, we obtain

$$\sum_{i=0}^{m-1} (-1)^i s^{(m-i-1)}(x) \frac{\partial^{m+i} R_y(x)}{\partial x^{m+i}} = \sum_{i=0}^{m-1} (-1)^i s^{(i)}(x) \frac{\partial^{2m-i-1} R_y(x)}{\partial x^{2m-i-1}}. \tag{A.4}$$

Therefore,

$$(s(x),R_y(x))_m=\sum_{i=0}^{m-1}s^{(i)}(0)\left[\frac{\partial^i R_y(0)}{\partial x^i}-(-1)^{(m-i-1)}\frac{\partial^{2m-i-1}R_y(0)}{\partial x^{2m-i-1}}\right]$$
$$+\sum_{i=0}^{m-1}(-1)^{(m-i-1)}s^{(i)}(1)\frac{\partial^{2m-i-1}R_y(1)}{\partial x^{2m-i-1}} \tag{A.5}$$
$$+(-1)^m\int_0^1 s(x)\frac{\partial^{2m}R_y(x)}{\partial x^{2m}}dx.$$

By Eq. (A.1), R_y satisfies

$$\begin{cases}(-1)^m\dfrac{\partial^{2m}R_y(x)}{\partial x^{2m}}=\partial(x-y),\\ \dfrac{\partial^i R_y(0)}{\partial x^i}-(-1)^{(m-i-1)}\dfrac{\partial^{2m-i-1}R_y(0)}{\partial x^{2m-i-1}}=0,\\ \dfrac{\partial^{2m-i-1}R_y(1)}{\partial x^{2m-i-1}}=0,\quad i=0,1,\ldots,m-1.\end{cases} \tag{A.3}$$

In case of $x\neq y$, R_y satisfies

$$(-1)^m\frac{\partial^{2m}R_y(x)}{\partial x^{2m}}=0, \tag{A.4}$$

with the boundary conditions

$$\begin{cases}\dfrac{\partial^i R_y(0)}{\partial x^i}-(-1)^{(m-i-1)}\dfrac{\partial^{2m-i-1}R_y(0)}{\partial x^{2m-i-1}}=0,\\ \dfrac{\partial^{2m-i-1}R_y(1)}{\partial x^{2m-i-1}}=0,\quad i=0,1,\ldots,m-1.\end{cases} \tag{A.5}$$

Equation $\lambda^{2m}=0$, is known as the characteristic equation of Eq. (A.4) with $2m$ eigenvalue multiplicity for $\lambda=0$. Hence, Eq. (A.3) has the following general solution

$$R_y(x)=\begin{cases}lR_y(x)=\sum_{i=1}^{2m}c_i(y)x^{i-1},\quad x<y,\\ rR_y(x)=\sum_{i=1}^{2m}d_i(y)x^{i-1},\quad x\geq y.\end{cases} \tag{A.6}$$

Since

$$(-1)^m\frac{\partial^{2m}R_y(x)}{\partial x^{2m}}=\partial(x-y), \tag{A.7}$$

we conclude

$$\frac{\partial^{2m-1}rR_y(y^+)}{\partial x^{2m-1}}=\frac{\partial^{2m-1}lR_y(y^-)}{\partial x^{2m-1}},\quad i=0,1,\ldots,2m-2, \tag{A.8}$$

and

$$(-1)^m\left(\frac{\partial^{2m-1} rR_y(y^+)}{\partial x^{2m-1}}-\frac{\partial^{2m-1} lR_y(y^-)}{\partial x^{2m-1}}\right)=1. \tag{A.9}$$

Eqs. (A.8), (A.9), and $2m$ equations from (A.5) are coupled for computing $4m$ unknowns $c_i(y)$ and $d_i(y)$, $i=1,2,\ldots,2m$, in (A.6). Beyrami et al. [37] presented the Mathematica source code of the above equations.

Spouse that ψ_i, $j=1,\ldots,N$, have been determined by Eq. (2.12). Throughout what follows, calculation of the approximate solution s_n in Eq. (2.14) is described. Let $\boldsymbol{\beta}_i^*=(\beta_{i,1}^*,\beta_{i,2}^*,\ldots,\beta_{i,i}^*)^T$ denote the solution of the following linear system,

$$\begin{bmatrix} (\psi_1,\psi_1)_m & (\psi_1,\psi_2)_m & \cdots & (\psi_1,\psi_{i-1})_m \\ (\psi_2,\psi_i)_m & (\psi_2,\psi_2)_m & \cdots & (\psi_2,\psi_{i-1})_m \\ \vdots & \vdots & \ddots & \vdots \\ (\psi_{i-1},\psi_1)_m & (\psi_{i-1},\psi_2)_m & \cdots & (\psi_{i-1},\psi_{i-1})_m \end{bmatrix}\begin{bmatrix} \beta_{i,1}^* \\ \beta_{i,2}^* \\ \vdots \\ \beta_{i,i-1}^* \end{bmatrix}=-\begin{bmatrix} (\psi_1,\psi_i)_m \\ (\psi_2,\psi_i)_m \\ \vdots \\ (\psi_{i-1},\psi_i)_m \end{bmatrix}, \tag{A.10}$$

and $\beta_{i,i}^*=1$. Let $\mathbf{A}$ denote the coefficient matrix of the above linear system. In order to get the entries of $\mathbf{A}$, using the integral operator in Eq. (2.4), we define L as

$$(Ls)(x)=\int_0^x K(x,t)s(t)t, \quad 0\le x\le 1, \tag{A.11}$$

$\mathbf{A}$ is Hermitian matrix and its entries can be obtained by

$$\begin{aligned}(\psi_i(x),\psi_j(x))_m &= (\psi_i(x),[L_y R_x(y)](x_j))_m \\ &= [\bar{L}_y(\psi_i(x),R_x(y))_m](x_j) \\ &= [\bar{L}_y\psi_i(y)](x_j).\end{aligned} \tag{A.12}$$

We define $\boldsymbol{\beta}_i=\dfrac{\beta_i^*}{\left\|\beta_i^*\right\|_m}$. In order to get the solution s_N, we proceed as follow. Let $\gamma_{i,k}=(\psi_i,\bar{\psi}_k)_m$ denote the coefficients of the following Fourier series,

$$\psi_i=\sum_{k=1}^{i-1}\gamma_{i,k}\bar{\psi}_k+\gamma_{i,i}\bar{\psi}_i. \tag{A.13}$$

Hence, we have

$$(\psi_i,\psi_i)_m=\sum_{k=1}^{i-1}\gamma_{i,k}^2+\gamma_{i,i}^2,$$

and

$$\gamma_{i,i}^2=\sum_{k=1}^{i-1}\gamma_{i,k}^2-(\psi_i,\psi_i)_m,$$

We denote the matrix form of the Eq. (A.13) as $\boldsymbol{\xi}=\boldsymbol{\Gamma}\bar{\boldsymbol{\xi}}$, where $\boldsymbol{\xi}=[\psi_1,\psi_2,\ldots,\psi_N]^T$, $\bar{\boldsymbol{\xi}}=[\bar{\psi}_1,\bar{\psi}_2,\ldots,\bar{\psi}_N]^T$, and $\boldsymbol{\Gamma}=[\gamma_{i,j}]_{i,j=1}^N$ is a lower triangular matrix. For lower triangular matrix $\mathbf{B}$,

whose ith row is $\boldsymbol{\beta}_i^T$, we have $\boldsymbol{\Gamma}\mathbf{B}=\mathbf{I}$, where $\mathbf{I}$ is the identity matrix. In what follows, c source code of the above procedure is presented.

```
void CalcBeta()
{
	double sum;
	for (int i = 0; i <= N - 1; i++)
	{
		for (int k = 0; k < i; k++)
		{
			BETA[i][k] = 0.0;
			for (int q = 0; q <= k; q++)
				BETA[i][k] += Beta[k][q] * A[i][q];
		}
		sum = 0.0;
		for (int q = 0; q < i; q++)
			sum += pow(BETA[i][q], 2.0);

		Beta[i][i] = 1.0 / (sqrt(A[i][i] - sum));

		for (int j = 0; j < i; j++)
		{
			sum = 0.0;
			for (int q = j; q <= i - 1; q++)
				sum += BETA[i][q] * Beta[q][j];
			Beta[i][j] = Beta[i][i] * (-sum);
		}
	}
}

double yn(double x)
{
	double result = 0.0;
	for (int i = 0; i < N; i++)
		for (int k = 0; k <= i; k++)
			result += Beta[i][k] * f(k) * SaiBar(i, x);
	return result;
}
```

Nomenclature

Latin		**Greek**	
r	Radial distance from the centrifuge axis to an arbitrary point in the centrifuge sore	ρ	Phase mass density
r_1	r at the inner core face	$\Delta\rho$	Difference between the phase densities
r_2	r at the outer core face	ω	Centrifuge angular velocity
Pc	Capillary pressure	β_{jk}	Gram–Schmidt orthogonalization coefficients
Pc_1	Capillary pressure at r_1	ψ_j	Base functions of W^m
Pc_2	Capillary pressure at r_2	$\bar{\psi}_j$	Orthonormal base functions of W^m
$Pc_{\max}$	maximum capillary pressure	S	Wetting phase saturation defined on $[0, Pc_{\max}]$, i.e. $s(Pc_1)$ where $0 \le Pc_1 \le Pc_{\max}$

S	Wetting phase saturation defined on $[0, Pc_{\max}]$, i.e. $S(Pc_1)$ where $0 \le Pc_1 \le 1$	S_n	Approximate value of wetting phase saturation defined on $\left[0, Pc_{\max}\right]$
$\overline{S}$	Average wetting phase saturation defined on $[0, Pc_{\max}]$	**Metric Units**	
B	Dimensionless factor, $B = 1-(r_2 / r_1)^2$ for drainage and $B = 1-(r_1 / r_2)^2$ for imbibition	Pc	pascal
F	Known side of the Volterra integral equation defined on $[0, Pc_{\max}]$	r	Meter (m)
K	Kernel of the Volterra integral operator	ρ	Kgr/m^3
f	Known side of the Volterra integral equation defined on [0, 1]	ω	Radian per second
s	Wetting phase saturation defined on $\left[0,1\right]$, i.e. $s(Pc_1)$ where $0 \le Pc_1 \le 1$		
s_n	Approximate value of wetting phase saturation defined on $\left[0,1\right]$		

References

1. Andersen, P. "Capillary Pressure Effects on Estimating the Enhanced-Oil-Recovery Potential During Low-Salinity and Smart Waterflooding", SPE J., **25** , pp. 481–496 (2020).
2. Pettersson, K., Maggiolo, D., Sasic, S., Johansson, P., and Kalagasidis, A. S., 2021. "Contribution of dynamic capillary pressure to rainfall infiltration in thin homogeneous growth substrates", Journal of Hydrology, **603**, Part A, 126851 (2021).
3. Lasseux, D., and Valdés-Parada, F. J. "Upscaled dynamic capillary pressure for two-phase flow in porous media", Journal of Fluid Mechanics, **959**, pp. 1-12 (2023).
4. Zankoor, A., Khishvand, M., and Piri, M. "In-Situ Capillary Pressure and Its Interrelationships with Flow Characteristics During Steady-State Three-Phase Flow in Water-Wet Berea Sandstone", Water Resources Research, **58**, e2022WR032976 (2022).
5. Li, Y., Li, H., Chen, Sh., Luo, H., and Liu, C. "Investigation of the dynamic capillary pressure during displacement process in fractured tight rocks", AIChE journal, **66**, e16783 (2020).
6. Oktaviany, A. P. P., Pramana, A. A., Farahdibah, U., Maharsi, D. A., Astuti, W., and Gibrata, M. A. "Digital Core Analysis of Capillary Pressure in Sandstone", Scientific Contributions Oil & Gas, **45**, pp. 183 – 191 (2022).
7. Lin, Q., Bijeljic, B., Raeini, A. Q., Rieke, H., and Blunt, M. J. "Drainage Capillary Pressure Distribution and Fluid Displacement in a Heterogeneous Laminated Sandstone", Geophysical Research Letters, **48**, e2021GL093604 (2021).
8. Xu, W., Huang, H., Ke, Shi-Z., Li, Jin-P., Zhang, Hai-F., and Hu, Yu-B. "An integral method for calculation of capillary pressure based on centrifuge data of tight sandstone", Petroleum Science, **19**, pp. 91-99 (2022).
9. Foroughi, S., Bijeljic, B., and Blunt, M. J. "A Closed-Form Equation for Capillary Pressure in Porous Media for All Wettabilities", Transport in Porous Media, **145**, pp. 683–696 (2022).
10. Bursey, B. J., Mohagheghian, E., Sripal, E., and James, L. A. "Prediction of centrifuge capillary pressure using machine learning techniques", E3S Web of Conferences **367**, 01004, pp. 1-11 (2023).

11. Brunner, H. “Collocation Methods for Volterra Integral and Related Functional Equations”, Cambridge Monographs on Applied and Computational Mathematics, Cambridge University Press, (2004), ISBN9780511543234.
12. Hermansen, H., Eliassen, O., Guo, Y., and Skjaeveland, S.M. “Capillary pressure from centrifuge – A new direct method”, Conference: Second European Core Analysis Symposium (Eurocas II), London, UK, pp. 453–468 (1991).
13. Glotin, J., Genet, J., and Klein, P. “Computation of drainage and imbibition capillary pressure curves from centrifuge experiments”, SPE-20502-MS, presented at the SPE Annual Technical Conference and Exhibition, New Orleans, Louisiana, pp. 313-324 (1990).
14. Hassler, G. L., and Brunner, E. “Measurements of capillary pressure in small core samples”, Trans. AIME, **160**, pp. 114–123 (1945).
15. Forbes, P.L. “Centrifuge Data Analysis Techniques: A SCA Survey on the Calculation of Drainage Capillary Pressure Curves from Centrifuge Measurements”, A Report published by the Society of Core Analysts, p. 184 (1997).
16. Hoffman, R.N. “A technique for the determination of capillary pressure curves using a constantly accelerated centrifuge”, SPE J., **3**, pp.227–235 (1963).
17. van Domselaar, H. R. “An exact equation to calculate actual saturations from centrifuge capillary pressure measurements”, Revista Tecnica Intevep, **4**, pp. 55–62 (1984).
18. Rajan, R. R. “Theoretically correct analytical solution for calculating capillary pressure-saturation from centrifuge experiments”, SPWLA-1986-J, presented at the SPWLA 27th Annual Logging Symposium, Houston, Texas, pp. 1–17 (1986).
19. Forbes, P. L. “Simple and accurate methods for converting centrifuge data into drainage and imbibition capillary pressure curves”, The Log Analyst, **35**, pp. 31–53 (1994).
20. Nazari Moghaddam, R. “A rapid and accurate method for calculation of capillary pressure from centrifuge data”, Journal of Petroleum Science and Engineering, **135**, pp. 577-582 (2015).
21. Subbey, S., and Nordtvedt, J. -E. “Capillary pressure curves from centrifuge data: A semi-iterative approach”, Computational Geosciences, **6**, pp. 207–224 (2002).
22. Fernø, M. A., Bull, Ø., Sukka, P. O., and Graue, A. “Capillary pressures by fluid saturation profile measurements during centrifuge rotation”, Transport in Porous Media, **80**, 253–267 (2009).
23. Zaremba, S. “Sur le calcul numerique des fonctions demandees dans le probleme de Dirichlet et le probleme hydrodynamique”, Imprimerie de l'Universite, 70 pages (1909).
24. Beyrami, H., Lotfi, T., and Mahdiani, K. “Stability and error analysis of the reproducing kernel Hilbert space method for the solution of weakly singular Volterra integral equation on graded mesh”, Applied Numerical Mathematics, **120**, pp. 197–214 (2017).
25. Aronszajn, N. “Theory of reproducing kernels”, Transactions of the American Mathematical Society, **68**, pp. 337–404 (1950).
26. Cui, M., and Lin, Y. “Nonlinear Numerical Analysis in Reproducing Kernel Space”, Nova Science Publishers, United States, (2009), ISBN:978-1-60456-468-6.
27. Karatas Akgül, E. “Reproducing kernel Hilbert space method for nonlinear boundary-value problems”, Mathematical Methods in the Applied Sciences, **41**, pp. 9142-9151 (2018).
28. Foroutan, M., Asadi, R., Ebadian A. ”A reproducing kernel Hilbert space method for solving the nonlinear three-point boundary value problems”, International Journal of Numerical Modelling: Electronic Networks, Devices and Fields, **32**, e2573 (2019).
29. Maleknejad, Kh., Hoseingholipour, A. “Numerical treatment of singular integral equation in unbounded domain”, International Journal of Computer Mathematics, **98**, pp. 1633-1647 (2021).
30. Micula, S. “A Numerical Method for Weakly Singular Nonlinear Volterra Integral Equations of the Second Kind”, Symmetry, **12**, 1862, pp. 1-15 (2020).

31. Attia, N., Akgül, A., Seba, D., Nour, A., and Riaz, M. B. “Reproducing kernel Hilbert space method for solving fractal fractional differential equations”, Results in Physics, **35**, 105225 (2022).
32. Bertsimas, D., and Koduri, N. “Data-Driven Optimization: A Reproducing Kernel Hilbert Space Approach”, Operations Research, **70**, pp. 3-8 (2021).
33. Tuo, R., He, Sh., Pourhabib, A., Ding, Y., and Huang, J. Z. “A Reproducing Kernel Hilbert Space Approach to Functional Calibration of Computer Models”, Journal of the American Statistical Association, **118**, pp. 883-897 (2023).
34. Abbasbandy, S., and Khodabandehlo, H. R. “Application of reproducing kernel Hilbert space method for generalized 1-D linear telegraph equation”, International Journal of Nonlinear Analysis and Applications, **13**, pp. 485-497 (2022).
35. Pylak, D., and Wójcik, P. “Approximate Solution of a Dominant Singular Integral Equation with Conjugation”, Ukrainian Mathematical Journal, **73**, pp. 1495–1504 (2022).
36. Attia, N., Akgül, A. “A reproducing kernel Hilbert space method for nonlinear partial differential equations: applications to physical equations”, Physica Scripta, **97**, 104001 (2022).
37. Beyrami, H., Lotfi, T., and Mahdiani, K. “A new efficient method with error analysis for solving the second kind Fredholm integral equation with Cauchy kernel”, Journal of Computational and Applied Mathematics, **300**, pp. 385–399 (2016).

Figure 1: Centrifuge experiment setup: (a) drainage and (b) imbibition experiment setup.

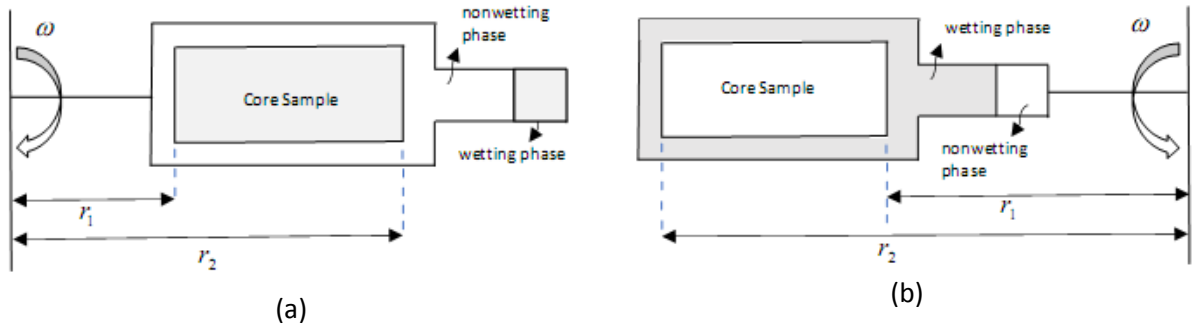

Figure 2: (a) Exact and local saturation obtained by RKHS method for Example D1 with B=0.75 and n=5, 10, and 50 data points. (b) The relative error of obtained approximate solutions.

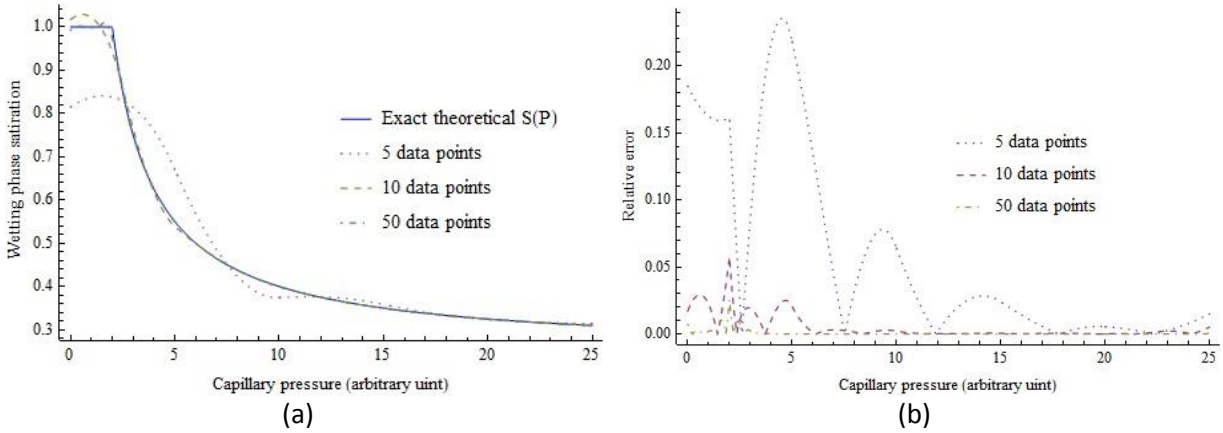

Figure 3: (a) Exact and local saturation obtained by RKHS method for Example D2 with B=0.75 and n=5,10,50 data points. (b) The relative error of obtained approximate solutions.

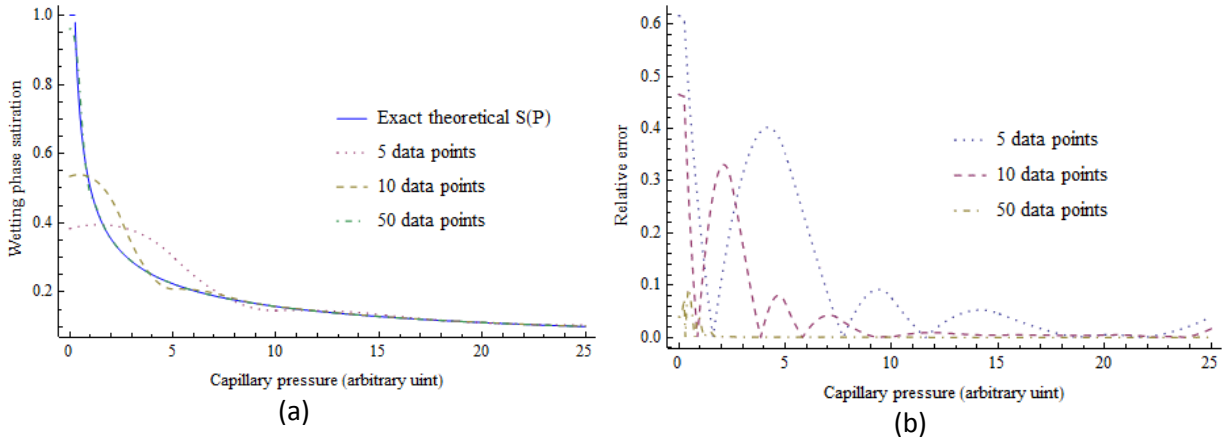

Figure 4: (a) Exact and local saturation obtained by RKHS method for Example D3 with B=0.75 and n=5, 10, and 50 data points. (b) The relative error of obtained approximate solutions.

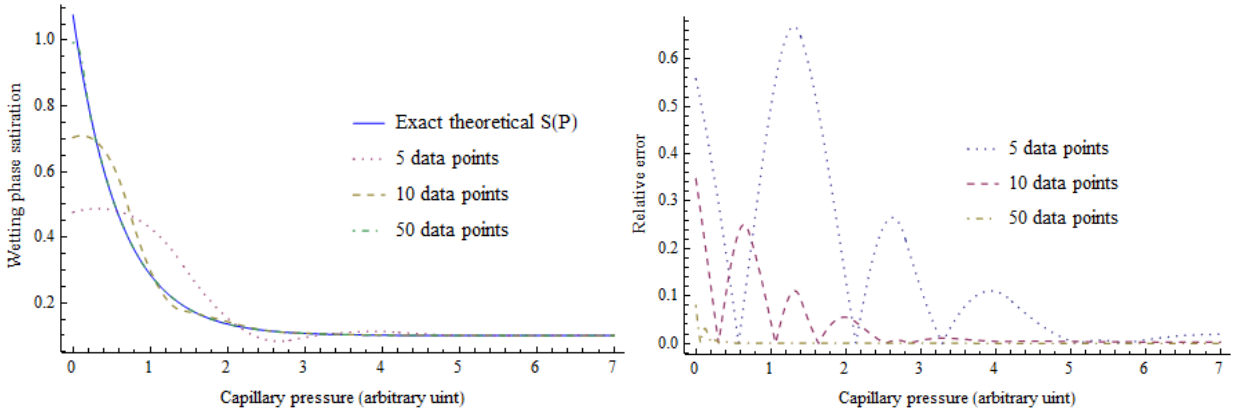

(a) (b)

Figure 5: (a) Comparison of local saturation obtained by RKHS and Forbes methods versus the exact function for Example D1 with B=0.75 and n=10 data points. (b) Interpretation of $S_B(Pc)$ *and* $\overline{S}_B(Pc_1)$ *for Example D1 with n=50 data points and B=0.1, 0.5, 0.8, 0.95, and 1.*

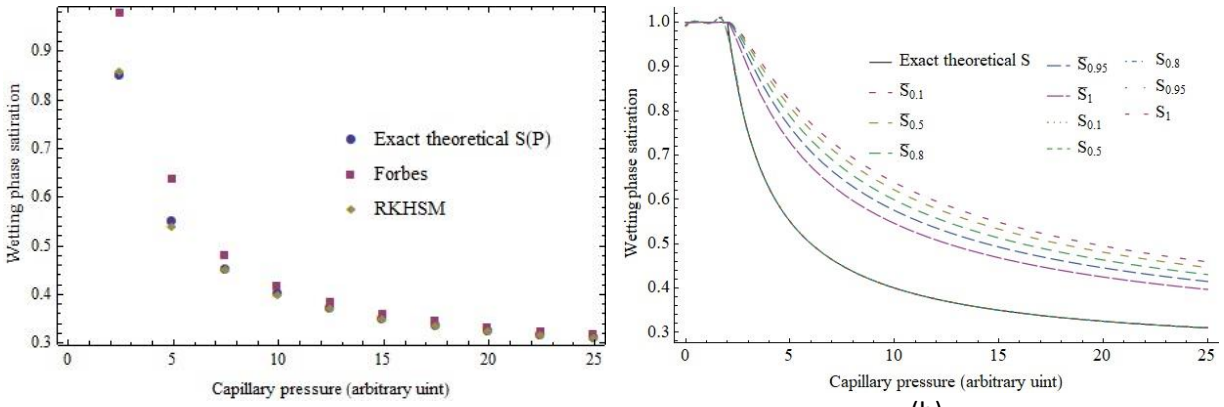

(a) (b)

Figure 6: (a) Comparison of local saturation obtained by RKHS and Forbes methods versus the exact function for Example D2 with B=0.75 and n=10 data points. (b) Interpretation of $S_B(Pc)$ *and* $\overline{S}_B(Pc_1)$ *for Example D2 with n=50 data points and B=0.1, 0.5, 0.8, 0.95, and 1.*

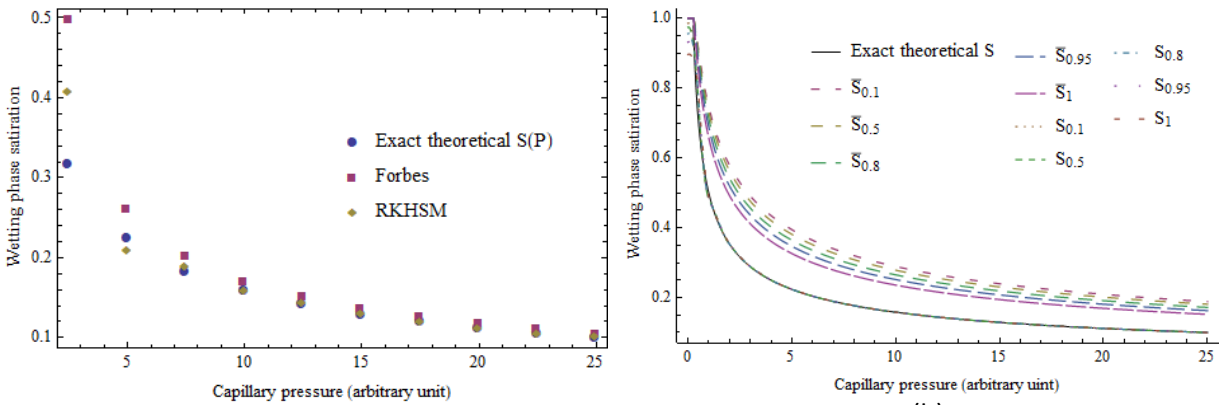

(a) (b)

Figure 7: (a) Comparison of local saturation obtained by RKHS and Forbes methods with the exact function for Example D3 with B=0.75 and n=10 data points. (b) Interpretation of $S_B(Pc)$ and $\overline{S}_B(Pc_1)$ for Example D3 with n=50 data points and B=0.1, 0.5, 0.8, 0.95, and 1.

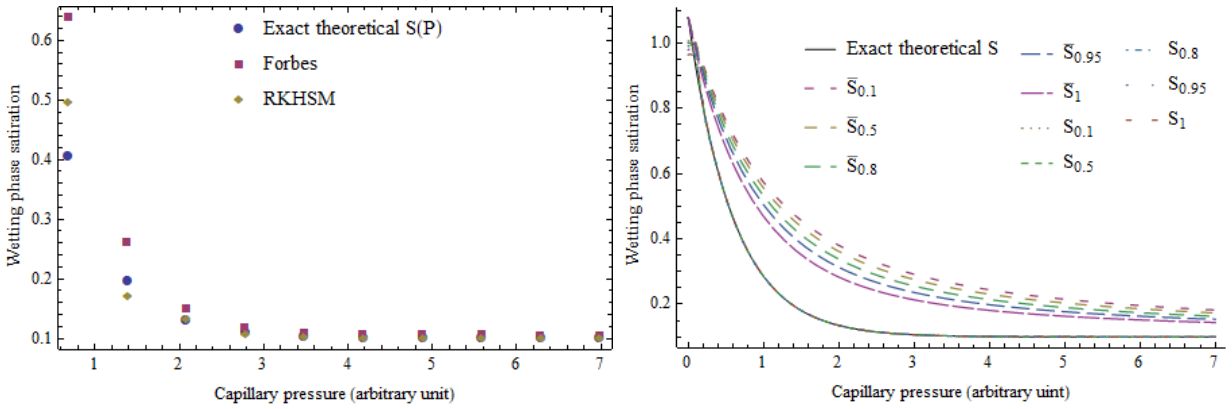

Figure 8: (a) Exact and local saturation obtained by RKHS method for Example I1 with B=-4.0 and n=5, 10, 50 data points. (b) The relative error of obtained approximate solutions.

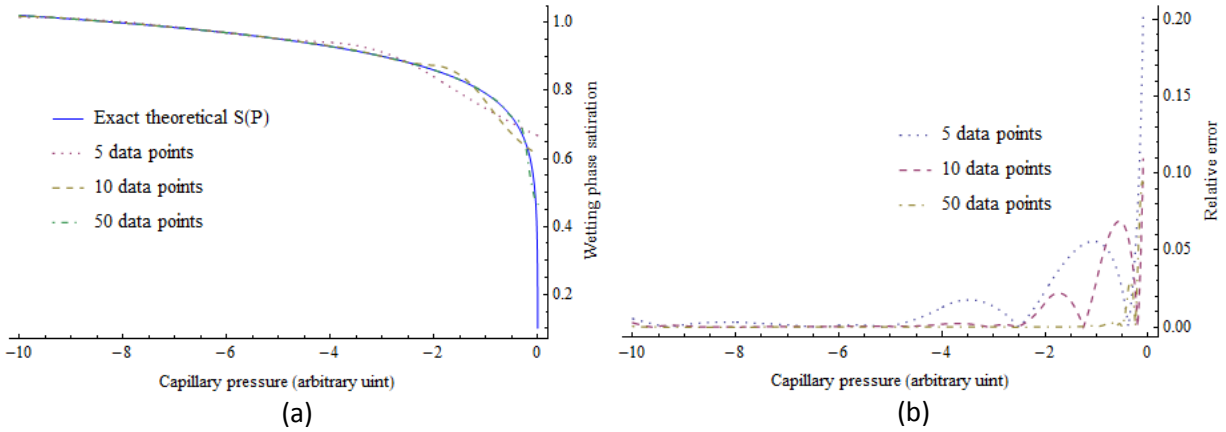

Figure 9: (a) Exact and local saturation obtained by RKHS method for Example I2 with B=-4.0 and n=5, 10, 50 data points. (b) The relative error of obtained approximate solutions.

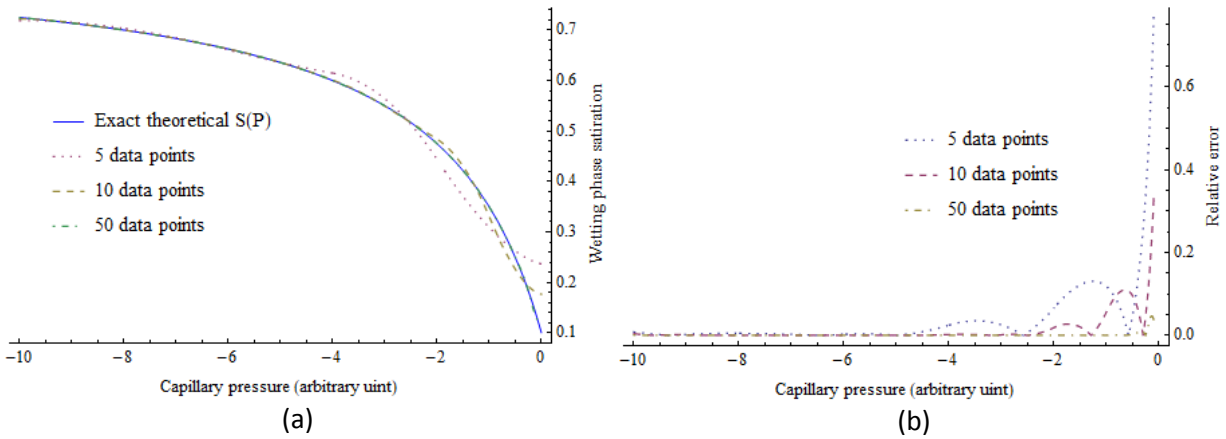

Figure 10: (a) Comparison of local saturation obtained by RKHS and Forbes methods with exact function for Example I1 with B=-4.0 and n=10 data points. (b) Interpretation of $S_B(Pc)$ *and* $\bar{S}_B(Pc_1)$ *for Example I1 with n=50 data points and B=-0.1, -1, -4, -20, and -100.*

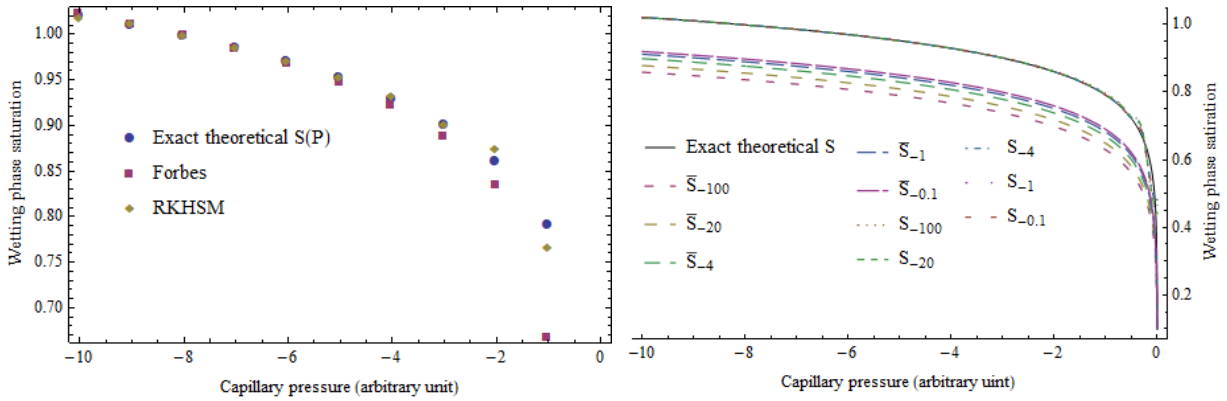

(a) (b)

Figure 11: (a) Comparison of local saturation obtained by RKHS and Forbes methods with exact function for Example I2 with B=-4.0 and n=10 data points. (b) Interpretation of $S_B(Pc)$ *and* $\bar{S}_B(Pc_1)$ *for Example I2 with n=50 data points and B=-0.1, -1, -4, -20, and -100.*

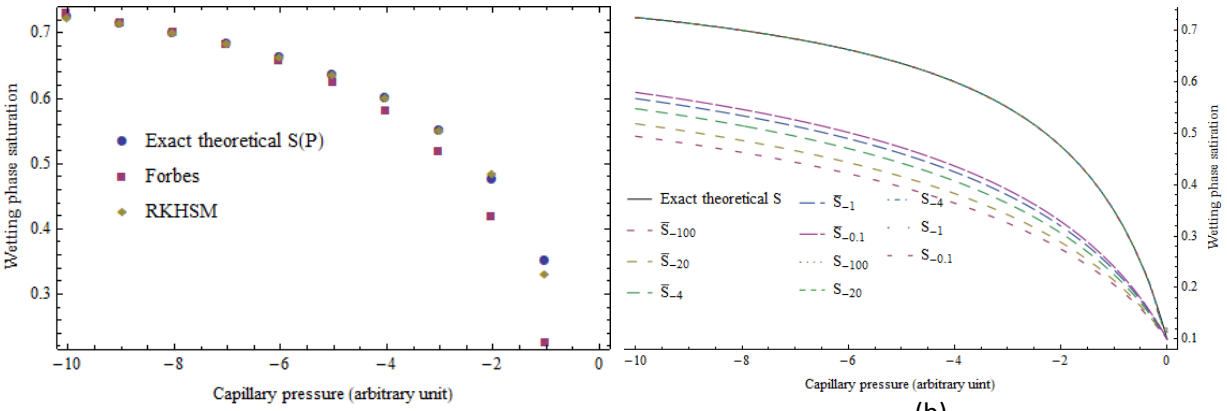

(a) (b)

Figure 12: (a) Interpretation of measured saturation for plug Example D4 where B=0.683148, based on RKHS and Forbes method for drainage experiment. (b) Interpretation of measured saturation for plug Example I3 where B=-1.06773, based on RKHS and the Forbes method for imbibition experiment.

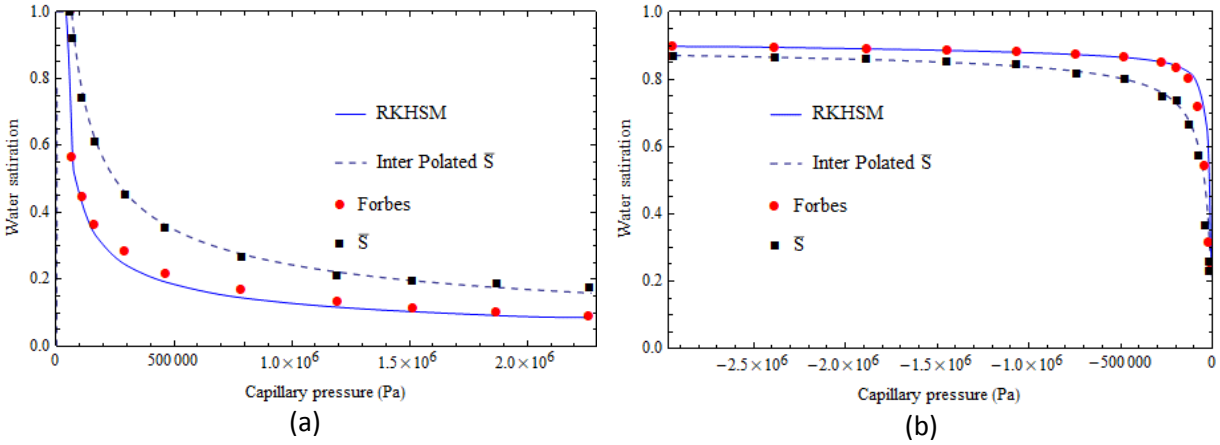

Table 1: The calculated RMSE of different methods for different drainage examples.

	ExamD1	**ExamD2**	**ExamD3**
HB [14]	0.184	0.118	0.158
NM [20]	0.048	0.059	0.088
Forbes [19]	0.053	0.062	0.080
RKHSM	4.91E-3	0.031	0.031

Table 2: The calculated RMSE of different methods for different drainage examples.

	ExamI1	**ExamI2**
Forbes [19]	0.041	0.047
RKHSM	9.41E-3	7.29E-3

Table 3: Rock sample properties of Example D4

Property	**Value**	**Unit**
Porosity	17.424	Percent
Absolute permeability	0.806	mD
Length	5.101	cm
Diameter	3.799	cm
Grain Density	2.836	gr/cc

Table 4: Rock sample properties of Example I3

Property	**Value**	**Unit**
Porosity	20.827	Percent
Absolute permeability	3.362	mD
Length	5.110	cm
Diameter	3.799	cm
Grain Density	2.851	gr/cc

Ehsan Kamari holds a B.S. degree from the Petroleum University of Technology, in 2003, and M.S. and Ph.D. degrees from Sharif University of Technology, in 2005 and 2012, respectively, all in Reservoir Engineering. He is now a project manager in the Department of Petroleum Engineering, Research Institute of Petroleum Industry (RIPI). His academic experience includes research on experimental and simulation studies of different EOR processes, micro-model experiments, and properties of oil reservoir rocks and fluids.

Hossein Beyrami was born in 1981 in Marand, Iran. He obtained his B.S. degree in Pure Mathematics from Payame Noor University of Tabriz, Iran, in 2004, he continued his studies into Applied Mathematics at Amirkabir University of Technology (Tehran Polytechnique), Tehran, Iran, and received his M.S. degree in 2007. He received his Ph.D. degree from Islamic Azad University, Science and Research Branch, Tehran, Iran, in 2016. He joined Research Institute of Petroleum Industry (RIPI), Tehran, Iran, in 2008, where he presently works as senior researcher. His research interests include: numerical simulation, optimization and software development.